IOP PUBLISHING EUROPEAN JOURNAL OF PHYSICS
Eur. J. Phys. **34** (2013) S51–S71 doi:10.1088/0143-0807/34/6/S51

The physics of near-infrared photography

Klaus Mangold[1], **Joseph A Shaw**[2] **and Michael Vollmer**[3,4]

[1] Ziegelhütte 9, Rottenburg, Germany
[2] Electrical Engineering, 610 Cobleigh Hall, Montana State University, Bozeman, MT 59717, USA
[3] Microsystem and Optical Technologies, University of Applied Sciences Brandenburg, Magdeburgerstr. 50, 14770 Brandenburg, Germany

E-mail: km@eye.de, jshaw@montana.edu and vollmer@fh-brandenburg.de

Received 4 June 2013, in final form 8 July 2013
Published 22 October 2013
Online at stacks.iop.org/EJP/34/S51

Abstract
The physics behind the sometimes strange effects and 'unnatural' appearance of near-infrared (NIR) photographs is discussed in terms of reflection, absorption and transmission of NIR radiation with the respective objects. Besides discussing how NIR cameras work, several visible and NIR photograph pairs are presented, which include vegetation, natural water, clouds, the sky, and humans. In addition, some physics-oriented experimental NIR images are presented which clearly demonstrate some of the basic physics behind some of these awesome sights.

(Some figures may appear in colour only in the online journal)

1. Introduction

Human perception is limited to the visible (VIS) spectral range that is defined by the luminous efficiency functions ranging between wavelengths of $\lambda = 380$ nm and $\lambda = 780$ nm. However, typical Si-based sensors in cameras and camcorders have sensitivities extending to about 1100 nm. In order to match the appearance of photographs to the human visual sensation, the near-infrared (NIR) part of the radiation incident on cameras is usually blocked by an IR cut-off filter. If this filter is removed, the incident radiation also contains the NIR, and the appearance of the resulting photographs changes. If an additional filter to block the VIS light is used, the modified camera then only detects NIR radiation, which can lead to strange effects in the appearance of photographs of well-known objects. These effects were at first only used by professional photographers, but the increasing availability of NIR-sensitive commercial consumer cameras (e.g., the so-called night shot options from Sony) has led many amateur photographers to explore the new realm of NIR photography.

It is quite easy to record NIR photographs; however, it can be difficult to understand why certain objects appear different in NIR light compared to the VIS range. Although

[4] Author to whom any correspondence should be addressed.

there are now quite a few books on conventional and digital IR photography on the market (e.g., [1–4]), one usually just finds qualitative arguments and descriptions of the effects, often without attempting to understand the underlying physics phenomena that give rise to the strange sights. This paper tries to fill part of the gap between awe and understanding of NIR photography by providing links between NIR photographs and the physics of NIR radiation interacting with matter. All spectra in this paper are recorded with either a commercial UV–VIS–NIR spectrometer Lambda 900 from Perkin Elmer or a mobile USB 2000 spectrometer from Ocean Optics.

1.1. NIR radiation: status quo in physics teaching

NIR photography is particularly interesting for physics teaching because it extends the visualization of physical phenomena beyond the VIS spectral range. This means it also allows the study of phenomena usually hidden from the eye. Similar visualization techniques that extend human vision are, e.g., high speed imaging, ultrasound imaging of objects below surfaces, medical imaging techniques such as x-rays, nuclear magnetic resonance imaging, positron electron tomography, as well as electron microscopies and many more examples.

In this paper we want to focus on extending our 'perception' only slightly beyond the VIS spectral range into the IR part of the spectrum, which offers many new physics phenomena and applications for study [5]. Although we will restrict ourselves to the NIR region from about 750 up to 1100 nm only, we mention that at even longer wavelengths, IR thermal imaging (usually in the ranges of 3–5 μm or 7 to 14 μm) with IR cameras has become a very prominent technique to study thermal radiation [6–9]. Short-wave IR cameras are also recently becoming more widely available, operating in the spectral range from about 0.9 to 1.7 μm.

Some aspects of NIR have already been applied to physics education, as can be seen from a number of publications [10–17]. They are all more or less from the last decade owing to the rapid development of low-cost camera technology, e.g. in the form of digital cameras, cell phones, camcorders and webcams, all of which use NIR-sensitive silicon-based detectors. The majority of cameras only passively detect NIR radiation, but some use an active scheme, often illuminating a scene with IR light emitting diodes (LEDs) and simultaneously detecting scattered NIR light [18]. They follow the tradition of early work, which used point detectors [19] to investigate NIR features for teaching purposes, e.g. visualizing the IR signals from remote control devices [20]. In addition to direct visualization, there are even some indirect visualization techniques available, such as using thermally sensitive materials [21, 22]. To the best of our knowledge, so far, there has been no study devoted to the teaching and learning issues in the field of NIR physics, dealing, e.g., with the common difficulties encountered by students when studying this topic. We hope that this work may stimulate further research in this field. Finally, most of these reported examples deal with physics experiments and do not use the vast and much older field of IR photography.

1.2. Natural source of NIR radiation: the Sun

Figure 1 shows a typical spectrum of sunlight incident outside the atmosphere and at sea level for typical midlatitude continental conditions (e.g., near northern latitude 45°). These spectra demonstrate that outdoor NIR photography using the Sun as a light source will have no exposure problems at all: the spectral irradiance decreases only slightly with increasing wavelength, leaving ample radiation available for photography.

In the broad spectral range extending from the shortest VIS wavelengths near 400 nm (violet light) all the way through far IR wavelengths near 30 μm, solar irradiance at the

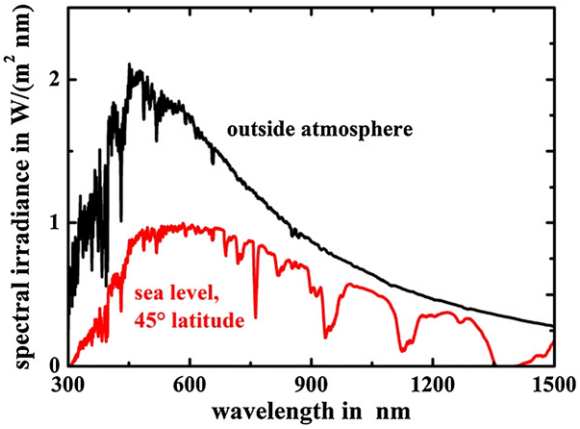

Figure 1. Typical example spectrum of available sunlight in the VIS and NIR region. Theoretical Modtran spectra (see [23]) calculated with 30 GHz frequency resolution (i.e., real spikes in UV), but smoothed in 3 THz bins, with a solar zenith angle of 45° for the 1976 US Standard Atmosphere at sea level (for a wavelength of 1000 nm, the 30 GHz and 3 THz intervals refer to wavelength intervals of 0.1 nm and 10 nm, respectively). The integral of the entire curve of solar irradiance at the mean Earth–Sun distance (outside Earth's atmosphere) yields approximately 1370 W m^{-2}.

mean Earth–Sun distance (W m^{-2} outside Earth's atmosphere) exhibits a spectrum that closely approximates a blackbody at a temperature of 5800–6000 K, with the approximation being especially valid for NIR and longer wavelengths [24]. In the ultraviolet region, the solar spectrum has many fine spectral features arising from emission and absorption in the gases that constitute the outer reaches of the solar atmosphere. When solar radiation penetrates into Earth's atmosphere, its spectrum is multiplied by the Earth's atmospheric transmission, which gives rise to many narrow and broad spectral features impressed upon the overall blackbody-like spectral shape, as shown in figure 1. From this figure we can conclude that spectral features of the solar light source should not lead to striking new features in relatively broadband NIR photographs.

2. Basics of NIR photography

2.1. Conventional early NIR photography

The appearance of natural and artificial objects around us when observed with the naked eye depends on the mechanisms of colour vision, which arise from the interplay of the signals of the various light receptors in the human eye and signal processing in the brain. Early photography created images from photochemical reactions with silver salt crystals embedded in films. Initially, no spectral selection could be made, and consequently only black-and-white images could be produced by the film. In order to get colour photographs, a number of different photosensitive layers plus colour filters were added in a stack, all of which together made the film emulsion. Obviously, the different colour-sensitive layers and the colour filters determined the spectral response of the film to incident light. One could, however, only get the same colour impression of a scene as observed with the eye if the overall emulsion spectral response, together with the subsequent development of the film, matched the eye's sensitivity.

Conventional films for black-and-white or colour photography usually had a spectral sensitivity between 370 and 700 nm. As such, they had no chance of detecting any NIR radiation. However, it was possible to create special IR-sensitive films that could operate up to wavelengths of about 850 nm. When combined with filters blocking the VIS part of the spectrum, it was possible to record images using radiation from a narrow spectral range of around 750–850 nm. Though possible, we may say that these films offered only very limited possibilities for studying NIR phenomena. One impressive example was the first IR image of a rainbow using such NIR film [25, 26], demonstrating that nature offers beautiful physics phenomena beyond the limits of our own sight.

2.2. NIR detection with modern digital cameras

The situation changed with the development of digital cameras. Nowadays, modern cameras have focal plane array image sensors (of either CCD or CMOS type) of typically around 10 megapixels or more. This means the detector itself contains millions of individual light detectors, each of which converts incident light to an electrical signal via the photoelectric effect. When light is incident on a detector pixel, the generated electrical signal is typically stored in a capacitor and the accumulated charge is a measure of the amount of incident radiation. Since the detectors are based on silicon, the typical sensitivity curves for each pixel are similar to the graph in figure 2(a), which depicts the sensitivity of a silicon photodiode. If expressed as quantum efficiency (i.e., the photon-to-electron conversion probability), typical modern CCD sensors have spectra as shown in figure 2(b). Both spectra clearly show the cut-off wavelength around 1100 nm, caused by the band gap in silicon of around 1.1 eV. The CCD sensor efficiencies differ from simple Si photodiodes since the CCD arrays have additional layers and gate electrodes which can selectively absorb radiation. Therefore sensitivity depends on whether the light must enter through more or fewer such layers as seen in figure 2(b) for front or back illumination. Using such detectors obviously means that even simple digital cameras are potentially able to detect NIR radiation.

Whether or not a digital camera does actually detect IR radiation depends largely on the spectral transmittance of colour filters and optics between the lens and the detector. For example, colour information is usually obtained in a consumer digital camera by covering the image sensor with a patterned array of red, green and blue colour filters in front of the detectors. As a consequence, a portion of the detectors respond to red, green and blue light, respectively, and the subsequent signals create colour images. (Alternatively, the incident light can be separated into the various colour components using dichroic prisms and illuminating three different CCD arrays, but these more expensive 'three-chip' or more complex systems will not be treated here.)

The use of silicon-based detectors with colour filters means that the colour within images from a digital camera depends on, first, the spectral response of individual detectors, second, the spectral transmission of the various colour filters, and third, the subsequent signal processing. Figure 2(c) depicts typical spectral response curves for the red, green and blue pixels of a detector chip, resembling the convolution of detector sensitivity and filter transmission.

Since cameras are normally used for VIS light photography, and because the NIR response introduces some effects which do not correspond to our normal visual perception (see examples in this paper), most camera manufacturers also include an IR blocking filter in the camera with transmission curves similar to the one in figure 3(a). Depending on their type, they can show interference oscillations as seen for one filter transmission curve in this figure. Additionally, there is usually a UV cut-off provided by the glass lenses, whose transmission falls off rapidly at wavelengths shorter than approximately 400 nm.

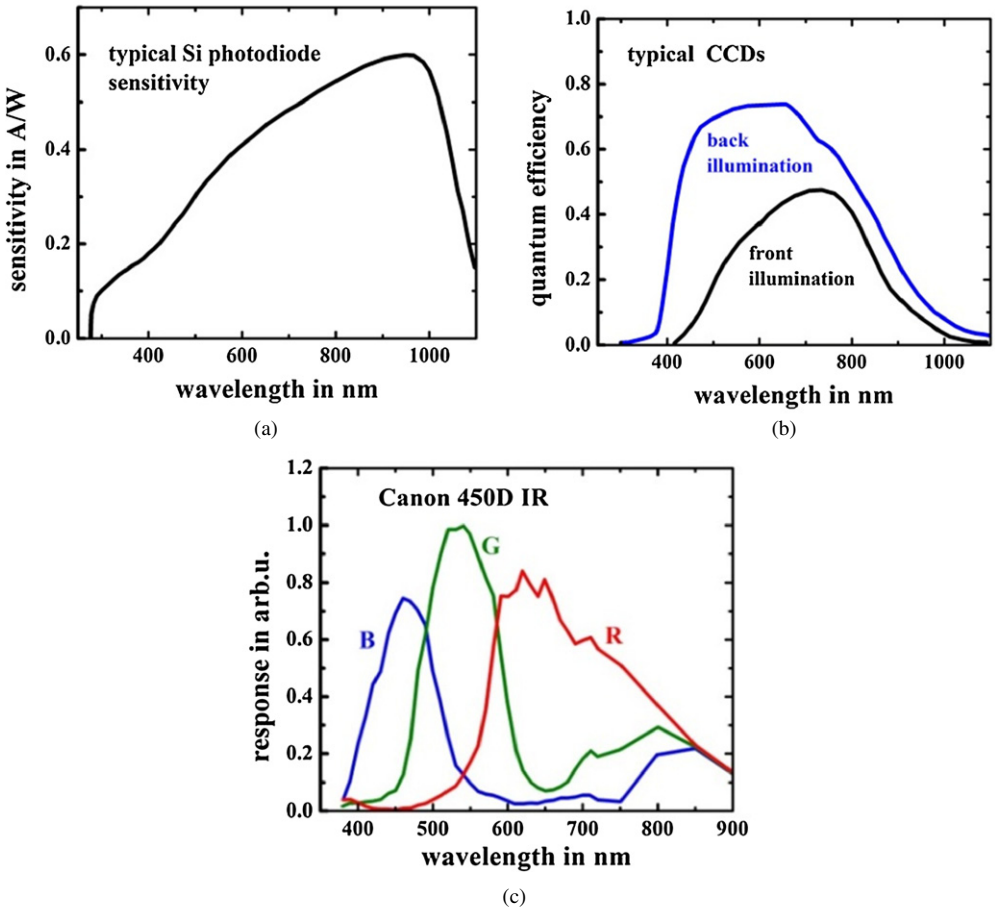

Figure 2. (a) Typical sensitivity spectrum of a silicon photodiode (after Hamamatsu S 2386). (b) Typical quantum efficiency spectra of modern CCD focal plane arrays as used in modern cameras (after Hamamatsu). Most cameras have less expensive front-illuminated CCD sensors, while specialized scientific cameras use the more efficient back-illuminated CCD sensors. (c) Typical detector sensitivity of a Canon EOS 450 DSLR without an IR-blocking filter (after Mauer [27]).

2.3. Modifications of VIS cameras for NIR photography

Concerning NIR photography, the obvious question is: how can one use commercial digital cameras, because they have an IR cut-off filter? Obviously, one must remove this filter and then insert other filters that can block all or part of the VIS spectrum. The inserted filter or glass is necessary, as it protects the sensor. The inside of a consumer-grade digital camera, with the detector and IR-blocking filter removed, is shown in figure 3(b). Unfortunately, opening the case of a digital camera results in invalidating its warranty, so only a specialist should perform the necessary camera modifications.

In the examples presented below, two different camera modifications were used. In the first one the IR-blocking filter was replaced with a glass plate with relatively constant transmission in the VIS and NIR region. Therefore the sensor was now exposed to radiation from below 400 nm up to about 2.5 μm, where the transmission of glass lenses falls to zero. Since the

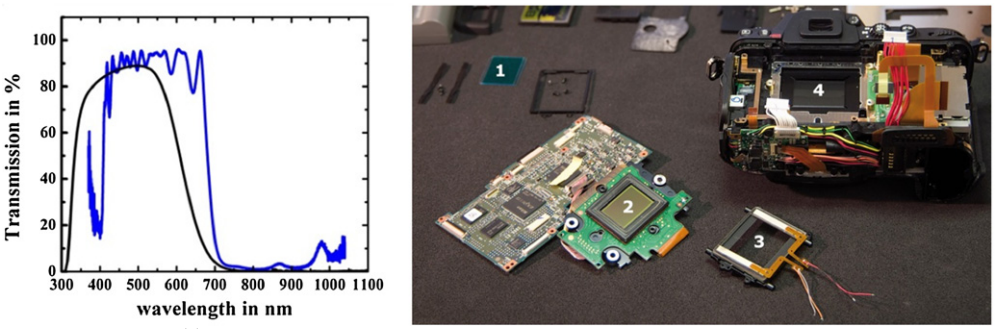

(a) (b)

Figure 3. (a) Example of two transmission spectra for the typical IR-blocking filters used in digital cameras. (b) Inner parts of a modern digital camera. Number (1) is the removed IR cut-off filter (and also low pass anti-aliasing filter), (2) the camera sensor of size $\approx$ 22.5 mm $\times$ 15.0 mm, (3) holder for the filters and (4) the shutter.

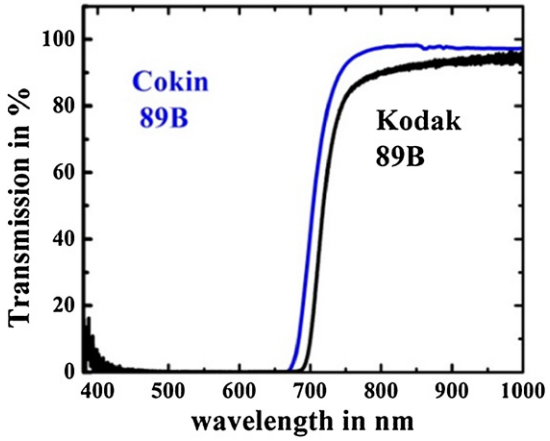

Figure 4. Typical transmission of NIR transmission filters, i.e. VIS blocking filters.

detector only responds to the spectral region below 1100 nm, this first modification resulted in a camera that detects VIS and NIR light. An added advantage of this approach is that more light is incident on the detector than in normal VIS-only imaging, which results in shorter exposure times.

The second modification used VIS-blocking filters for the VIS spectral range, with filter characteristics similar to the graph shown in figure 4. In this case, the digital camera was a true NIR camera and no longer could be used to record VIS images. Practical consequences of this type of modification are that the camera's automatic focusing or exposure mechanisms are no longer useful.

Whether the camera's auto exposure (AE) system works in the NIR depends on its design. Different AE schemes are available. Many of them use the image sensor to measure the incident light. This information is then used to control the exposure time, opening diameter of the iris, and electronic parameters such as the integration time of sensors and gain of amplifiers before

digitization. Depending on the algorithms used by the camera (which are optimized for VIS light), the AE system may or may not work in the NIR.

If desired, the first camera modification can allow even more flexibility through the use of various (larger size) cut-off filters in front of the camera lens. Most of the photographs presented in this paper have been recorded with a modification type 1 camera, which is able to detect VIS and NIR radiation. The choice of spectral range was then realized by placing appropriate (large) filters in front of the lens.

It is worthwhile mentioning that the two filters (figures 3(a) and 4) behave differently. The IR-blocking filter (figure 3(a)) is usually an interference filter, so its transmission spectrum can have ripples and can include a fairly significant 'out-of-band' peak near 980 nm, whereas the VIS-blocking long-pass filters may be either interference filters or absorbing filters, which often have fewer ripples, i.e. a smoother shape (for more details on filters, see [28]).

The typical IR filter in figure 4 still has some residual transmission in the red part of the VIS spectral range. However, since the luminous efficiency $V(\lambda)$ for photopic (i.e. daylight) vision is decreasing rapidly towards the red part of the spectrum, with $V(\lambda = 700) = 0.004$ (compared to the maximum sensitivity of 1.0 at $\lambda = 555$ nm), one often defines the lower limit of NIR photography as a wavelength of about 700 nm.

In the following, we show sets of images of a variety of different objects observed in the VIS range with a standard camera, as well as in NIR modification 1 (VIS+NIR) or NIR modification 2 (NIR only). For each object we discuss the respective differences in appearance arising from the underlying physics and, in particular, the differences in reflection and transmission spectra.

First, we discuss two major differences that are encountered when dealing with NIR photographs. Owing to the strong decrease in sensitivity towards longer wavelengths (figure 2), it is obvious that a much smaller amount of radiation will be detected by the camera sensors compared to VIS-image recording. There is no general rule for exposure time, which can vary quite widely depending on the camera used, and therefore this must be tested for any given conditions. Exposure time definitely will be longer than a VIS exposure time and usually a tripod is recommended. Second, if a VIS-blocking filter, such as the one shown in figure 4, is used, some tiny fraction of residual VIS radiation may enter the camera and produce a false colour image whose hue will depend on the chosen white balance. Such false colour IR photographs may be fascinating, but for a physics discussion it will often be easier to convert them into traditional black-and-white IR photographs using any common image editing program.

Our first examples are photographs of the filters themselves. Figure 5 depicts both VIS and NIR images of a NIR-blocking filter (having a faint blue tint) and a VIS-blocking filter (appearing black). Both were lying on a white piece of paper illuminated by daylight.

3. Selected examples

3.1. Vegetation and wood effect

When first recording NIR photographs in 1910, Wood wrote 'We obtain in this way photographs of objects taken by means of the IR radiations. They are quite different in appearance from ordinary photographs, their chief peculiarity lying in the intense blackness of the sky and the extreme brilliancy of the trees and grass. They resemble snow-covered landscapes in bright moonlight more than anything else' [29]. This description is probably still one of the best for describing the surprise and awe of looking for the first time at outdoor NIR photographs with green vegetation and blue skies. And in honour of his pioneering work on IR photography,

(a) (b)

Figure 5. VIS (a) and NIR (b) photographs of two typical filters, the left one blocking NIR and the right one blocking VIS light.

(a) (b)

Figure 6. Comparison of a conventional VIS photograph (a) and its corresponding NIR photograph (b) of the same scene recorded shortly afterwards as can be seen from the shadows (however, the lower left car moved in between the VIS and NIR photograph). Green vegetation appears spectacularly bright in the NIR and the contrast between sky and clouds is much higher compared to the VIS photograph (see text for details).

the effect that green vegetation looks extremely bright is called the Wood effect [30, 31]. Figures 6 and 7 show examples of conventional VIS photographs (a) and pure NIR photographs (b) of urban scenes containing houses, sky, clouds, and trees with green leaves. The most obvious differences are indeed much brighter vegetation, darker regions of clear sky, and higher contrast between clear sky and clouds. In addition, one may also detect reflections of the foreground trees in the windows of the house on the right-hand side of the photographs. These are much easier to see in the NIR since the leaves are a much brighter source of radiation there. We will come back to the sky and clouds later, but here we focus on the Wood effect.

Although Wood described the phenomenon of bright NIR scattering by vegetation, he did not explain it. This was done later by others, e.g. Mecke and Baldwin [32] (please note that we are not quite sure who was first to provide the now accepted interpretation), who called it the chlorophyll effect and referred to light path models within leaves from older work (see figure 8). According to this explanation, light enters the epidermis of leaves and is scattered in deeper sections where there are many cellular walls of interior cells separated by air inclusions. This model is strongly supported by ray tracing models [33]. Multiple scattering events finally give rise to very strong backscattering, similar to VIS light back-scattering from snow covered ground, where multiple scattering also leads to effective backscattering that yields very bright

(a) (b)

Figure 7. Another urban scene in VIS (a) and NIR (b) showing the same bright scattering effect of vegetation in the NIR. Note again the sky contrast and also the differences of reflection in the windows of the house on the right-hand side.

natural scenes. It has also been shown that the spectral distribution of backscattering depends on the tree species. For example, deciduous trees generally appear brighter than conifer trees in NIR images, even to the degree that hyper-spectral imaging can be used to classify different forests [34].

It is quite easy to verify the strong NIR backscattering in leaves by recording transmission and reflection spectra of sunlight through or from green vegetation. Figure 9 shows some examples of reflection spectra (R) and one transmission spectrum (T) for green leaves with either dull or shiny surfaces facing the spectrometer (shiny means a bit more specular in contrast to diffuse reflection). These spectra were recorded by using a mobile spectrometer whose detector only has a narrow detection angle. Therefore, scattered radiation at large angles is not detected and the resulting reflectance value is probably a bit lower than the hemispherical reflectance. This can be seen in comparison to hemispherical R and T measurements using a laboratory spectrometer (figure 10), where transmission and reflection in the NIR add up to 100% and absorption $A = 1 - R - T$ is only nonzero in the VIS range where chlorophyll absorbs.

It is obvious that the absorption features of chlorophyll, which are responsible for photosynthesis, are only important in the VIS spectral range. At NIR wavelengths, there is much less absorption and the high reflectivity is due to diffuse scattering of radiation from index of refraction inhomogeneities within the cells, such as interfaces due to cell membranes, water accumulation, etc. For leaves of 100–200 μm thickness, transmission can still be of

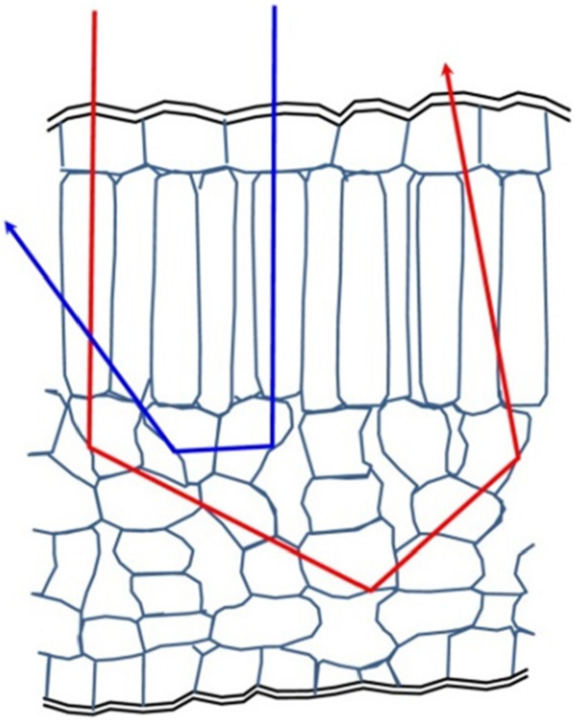

Figure 8. Scheme of light paths through leaves: after entering the leaf epidermis, light may be multiply scattered at the cellular walls in deeper regions (after [32]) as shown for two exemplary rays, the left one being scattered three times, the other one two times.

the order of 50% in the NIR range and a similar amount is scattered backwards. A biological consequence of high NIR reflectivity is that the plants will not heat up too much due to incident solar radiation, which is important for survival in hot climates. Interestingly, the NIR behaviour appears to be independent of the visual colour of the leaf (figure 10).

Because the difference of vegetation reflectance at VIS and NIR wavelengths depends strongly on chlorophyll content and plant health, it is readily possible to use red and NIR images to distinguish between healthy and unhealthy vegetation—even before such differences become apparent by eye. In fact, this method is used widely in the satellite remote sensing community to estimate vegetation health or crop water content, and to distinguish between vegetation and other land cover. One common method of doing this is with the normalized difference vegetation index (NDVI), computed as the difference of NIR − VIS reflectance, divided by the sum of NIR + VIS reflectance, as indicated in equation (1), in which R represents the measured scene reflectance in NIR and red bands.

$$\mathrm{NDVI} = \frac{R_{\mathrm{NIR}} - R_{\mathrm{red}}}{R_{\mathrm{NIR}} + R_{\mathrm{red}}}. \tag{1}$$

This concept has even been used recently to detect CO_2 gas leaking from underground with red and NIR imaging that measures changes in the NDVI of overlying vegetation. At the location of a gas leak, the higher soil gas concentration restricts the uptake of nutrients, leading to plant stress that is detectable in red and NIR image sequences [35, 36].

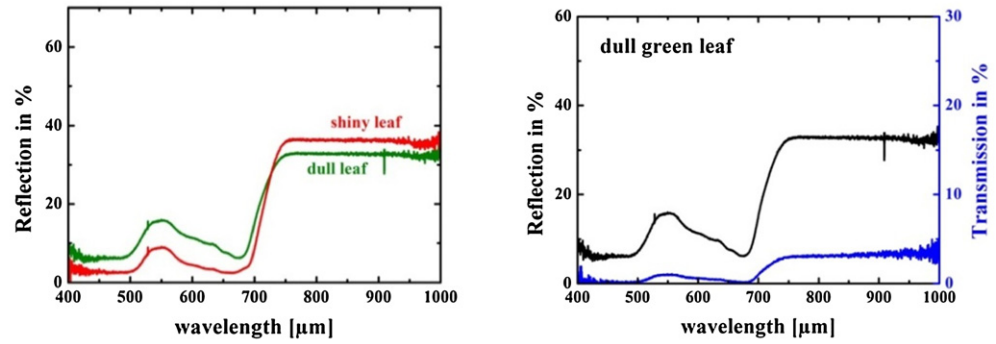

(a) (b)

(c) (d)

Figure 9. Reflection of a dull and a shiny leaf (a), reflection and transmission spectra from a dull green leaf (b), and VIS photographs of dull (c) and shiny (d) leaves. Spectra were recorded using a USB spectrometer at a reduced angular range.

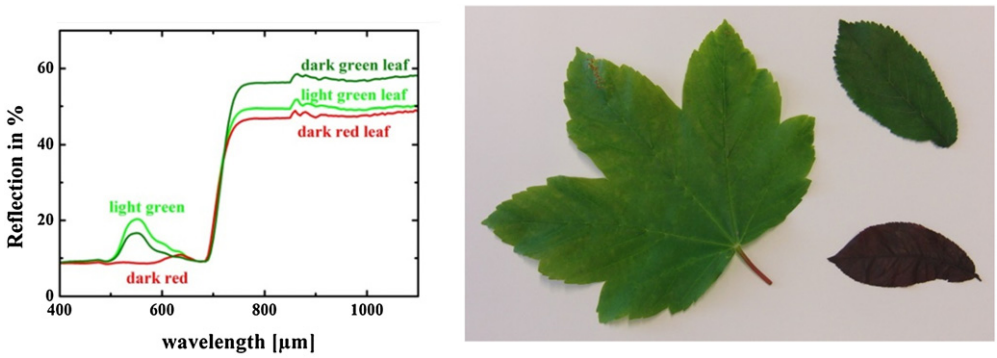

(a) (b)

Figure 10. (a) Reflection spectra of two green and one red leaf shown in (b), measured with an integrating sphere detector that gathered light from the complete backward hemisphere. The minimum thickness of the leaves was around 100 μm for the green and 200 μm for the red leaf. This resulted in approximately 30% max transmission near $\lambda = 550$ nm for the light green leaf, but only approximately 14% transmission at $\lambda = 640$ nm for the thicker red leaf.

(a) (b)

Figure 11. VIS (a) and NIR (b) images at a black-sand beach on the big island of Hawaii, recorded July 2000.

3.2. Blue sky, clouds, and haze

Besides the Wood effect, figures 6 and 7 also show partly cloudy and hazy skies. Similarly, figure 11 depicts a beach scene with a palm tree and mostly blue sky with some clouds and a bit of haze, recorded in Hawaii in July 2000 with a simple point-and-shoot camera fitted with an external VIS -blocking filter.

In this case, the camera had a sufficient NIR response so it was possible to use the same camera for VIS and NIR images simply by using and removing an external VIS-blocking filter; the VIS image was taken without an IR-blocking filter, and the NIR-image exposure time was more than ten times longer than the VIS-image exposure time.

These images again clearly show that vegetation has a much higher reflectance in the NIR. In addition and similar to figures 6 and 7, there is a much higher NIR contrast between the clear sky and the clouds. The reason lies in the scattering characteristics of molecules and the much larger haze or cloud droplets. The molecular scattering efficiency of atmospheric gases can be described by the Rayleigh law, i.e. a rapid $(1/\text{wavelength})^4$ falloff. In contrast, the scattering by much larger cloud droplets is described by Mie scattering, which has a more gradual reduction of scattering efficiency with wavelength. The consequence is a higher NIR contrast.

The contrast between dark clear sky and brighter clouds can also be understood more quantitatively from spectra of scattered sky light and diffusely scattered cloud light. Figure 12 depicts theoretical MODTRAN spectra of scattered light from a clear zenith sky (lower curve at long wavelengths) and an altostratus cloud (top curve at long wavelengths). Obviously, the clouds give rise to a much higher radiance (which describes the radiation input into a camera)

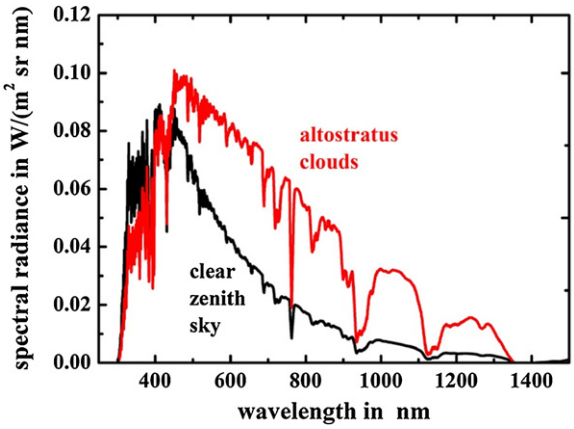

Figure 12. Spectra of scattered sunlight for a clear zenith sky and altostratus cloud calculated with Modtran [23] for solar zenith angle of 45° and the '1976 US Standard Atmosphere' model, which represents quite typical mid-latitude conditions that are relevant to much of the US and Europe. The simulated cloud was characterized by base at 2.4 km, top at 3.0 km, and total extinction of 128.1 km^{-1}, i.e. cloud optical depth is 0.6 km $\times$ 128.1 $km^{-1} = 76.9$.

in the NIR compared to the VIS spectral range. This means that clouds will have a much higher contrast in an NIR image compared to a VIS image, and that they will be imaged as bright and sometimes quite spectacular objects compared to the clear sky. The same also holds for thin clouds with much lower optical depth.

In addition, haze particles which scatter light according to Rayleigh's $(1/\lambda^4)$ law will scatter much less in the NIR than in the VIS spectral range. Therefore, NIR images were also considered helpful for the reduction of haze effects in photography [37].

3.3. Coloured liquids

Many liquids which have very dark colours in the VIS spectral range can appear colourless and highly transparent in the NIR. Figure 13 depicts an example of a bottle and a glass filled with a red wine. Three different images were recorded, one with normal IR cut-off filter ((a): for $\lambda = 400$–700 nm), another with an IR-transmitting filter ((c): for $\lambda = 830$–1100 nm), and one recorded with the whole spectral range from 400 to 1100 nm (b). The VIS image looks familiar, showing a deep red colour for the wine. In contrast, the NIR image makes the impression of a photograph of water in a glass and clear bottle recorded in black-and-white mode, i.e. both the red wine and the green glass have turned completely transparent in the NIR range. Detecting VIS plus NIR radiation simultaneously leads to a mixture of both: the green bottle still looks a bit green and the wine in the glass still has a red tint, though it is not very pronounced; i.e., the IR contribution dominates the appearance of the photograph. This is an excellent example of why IR cut-off filters are used in digital photography: any observer of the middle photograph would be extremely puzzled and at best expect to have wine mixed with water.

Figure 14 shows a similar scene recorded with VIS light only and NIR radiation only with a partially filled glass of Diet Coke. Again, the NIR photograph shows a more or less colourless liquid similar to water.

The explanation of this change from nearly opaque to transparent liquids is simple when studying transmission spectra of water compared to red wine and Diet Coke (figure 15).

(a) (b) (c)

Figure 13. Images of a bottle and glass filled with red wine recorded for VIS light only (a), whole range VIS and NIR (b) and IR only (c).

(a) (b)

Figure 14. Images of a glass partially filled with Diet Coke for VIS light only (a), and IR only (b).

Both Coke and red wine show strong absorption features in the VIS range with a steep (wine) or gradual (Coke) increase of transmission for longer wavelengths. This means that these liquids are becoming transparent for red light (giving the colour) and become highly transparent in the NIR.

In order to judge transmission quantitatively compared to water, all spectra in figure 15 were recorded with cuvettes of an inner length of 10 mm. Therefore, 100% transmission of water corresponds to no cuvette within the light path. Water is highly transparent in the VIS spectral range between 400 and around 800 nm. The observed maximum transmission is below 100%, in detail only slightly more than 90%. This is due to reflection losses which occur twice at the air–glass and twice at the water–glass interfaces. In the NIR spectral region there are absorption features around 950 and 1150 nm, and more beyond 1300 nm, leading to the dips in the water transmission spectrum.

Diet Coke and red wine spectra were recorded relative to the water curve in the figure, i.e. their 100% lines correspond to the case of pure water within the cuvette. The red wine

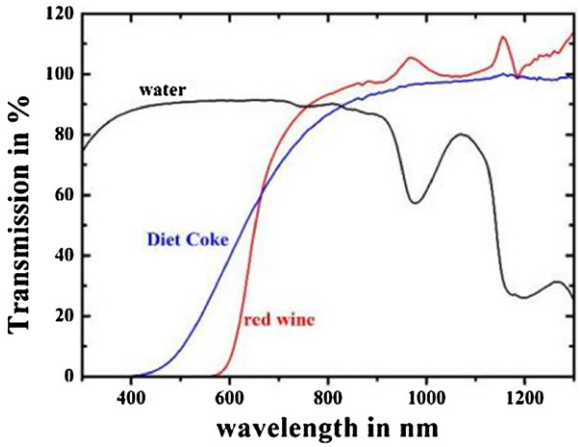

Figure 15. Transmission spectra of red wine, diet Coke and water, which explain the VIS, VIS + NIR and NIR images shown in figures 13 and 14 (see text for details).

reaches 100% transmission in the NIR around 850 nm. A good question to ask students is why the transmission of red wine can be larger than that of water, whereas Coke cannot. A hint to the answer is to refer to the spectrum of alcohol. Although ethanol has a similar spectrum as water, they differ slightly in their positions of maximum absorption and since wine has around 12% alcohol (i.e. less water), the spectra must differ.

The origin of the low VIS transmission differs for wine and Coke. The red wine colour stems from anthocyanins, which get their colour in low-pH surroundings (e.g. [38]), whereas the colour in Coke is due to so-called caramel colours [39].

Transmission spectra for Coke were recorded several times, immediately after opening the bottle with some gas bubbles still forming within the glass, and after all bubbles had dissipated. These spectra were mostly identical, exhibiting a gradual increase of transmission reaching 50% at around 600 nm and ending close to 100% in the NIR. The VIS part of this spectrum gives rise to the observed unsaturated colour of Coke. In contrast, deep red wine spectra usually start to rise in transmission at longer wavelengths, which gives a more saturated red colour because of near-perfect absorption of green and blue light. Spectra of Coke and wine both show a very strong transmission in the NIR, which explains the water-like appearance in the photograph.

The interested reader may try to perform similar experiments with other common everyday liquids such as coffee, etc. Even a very dark espresso can turn transparent in NIR images.

3.4. Visually opaque objects turning transparent in NIR

There are some objects, such as undeveloped photographic film, which are visually opaque but yet show high transmission in the NIR. This feature has already been used as a physics trick in demonstration experiments [18]. Figure 16 depicts a developed but unexposed roll (alternatively, one may use an undeveloped colour film roll) on top of a coloured paper photograph-bag recorded in VIS light and NIR radiation. In VIS light the film is opaque, whereas in the NIR it is highly transparent. In addition, it is obvious that the red and yellow coloured parts of the bag do not show up in the NIR image. This is easily understood from the transmission spectrum (figure 16(c)) of such film, which effectively blocks the VIS radiation.

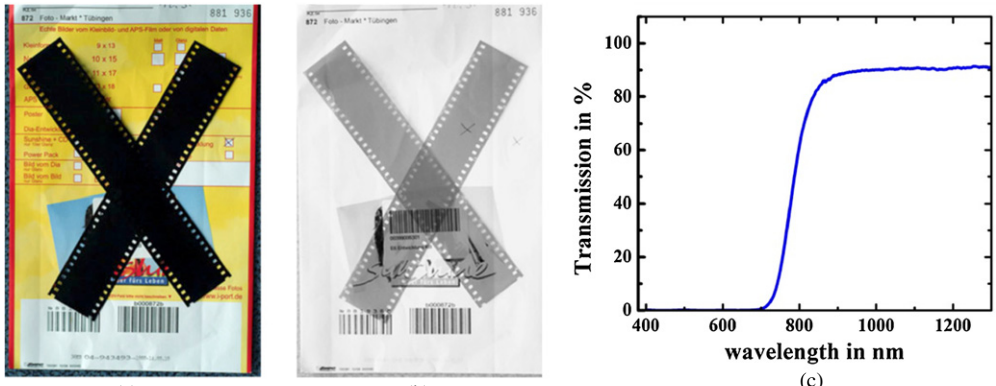

(a) (b) (c)

Figure 16. VIS (a) and NIR (b) images of two strips of developed but unexposed film, lying on top of a photograph-bag. Whereas the film strip is opaque for visible light, it is transparent for NIR radiation as shown by the spectrum (c).

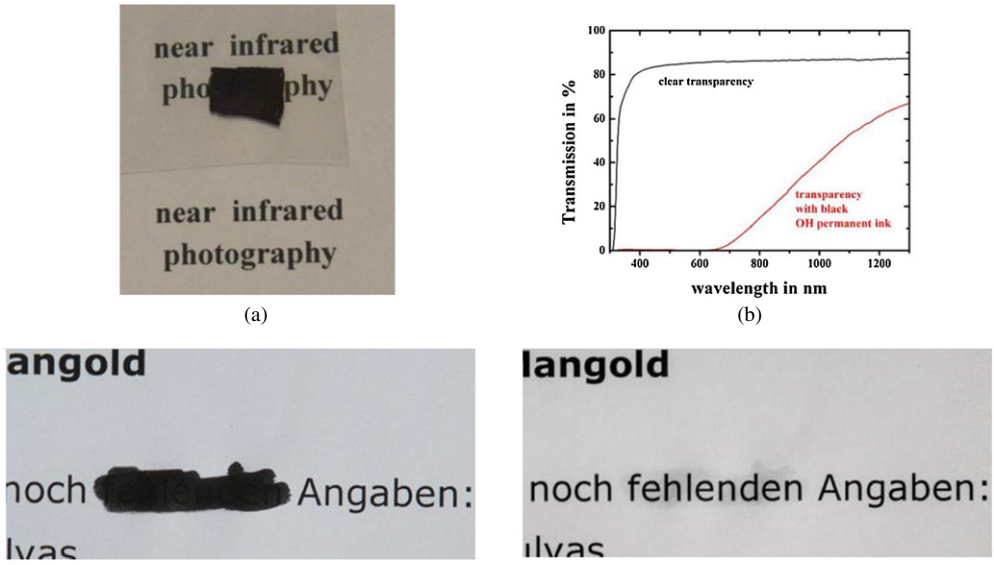

(a) (b) (c) (d)

Figure 17. (a) Example of black overhead marker on a transparency laid over black-and-white text on paper. (b) Spectra of a clear transparency as well as of part covered with the ink. (c) VIS image ($\lambda = 400$–700 nm) of some text covered directly with the black ink and (d) NIR image of the same text ($\lambda = 830$–1100 nm).

Since film rolls are no longer easily available, figure 17 shows the same phenomenon with a somewhat similar set up. One may just use standard transparencies used for demonstrations on overhead projectors and black overhead markers. The black ink from an overhead transparency marker makes it impossible to look through a transparency or—if marked on paper—to see the underlying text in the VIS spectral range (figure 17(a)). In contrast, this is possible in the NIR due to its transmission above 800 nm (figure 17(b)). Quite similarly, one may look

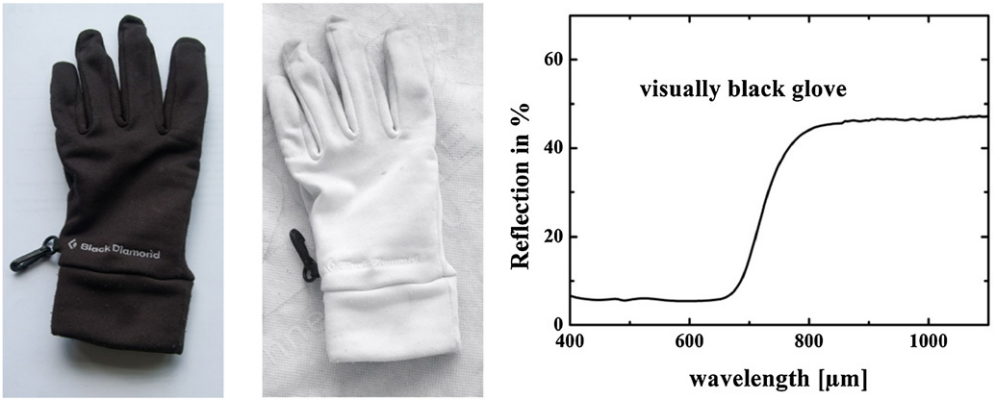

(a) (b) (c)

Figure 18. (a) visually black glove (made of 90% polyester and 10% Spandex) appears white in NIR (b). This is due to the diffuse scattering of the material reaching nearly 50% overall reflectivity (c).

directly through black ink on top of another text (figures 17(c), (d)) with NIR photographs. These examples can be demonstrated nicely in the classroom and sold as physics magic.

3.5. Some other visually black objects which become very bright in NIR

Synthetic fabrics are made of synthetic fibres consisting of long polymer molecular chains. Therefore, they are mostly white in the NIR, no matter what colour they have in VIS light (in cases where colorants are added for the VIS range). This most probably arises because most fibres are nonabsorbing in the NIR (their characteristic absorption features due to vibrational excitations of CH or CO bonds, etc, are usually at longer wavelengths); however, they scatter light strongly in all directions. This automatically yields large back- and forward-scattering contributions. In a way, this is similar to snow cover or clouds in the VIS spectral range.

Figure 18 depicts an example of a glove that appears black in the VIS but very bright in the NIR. Again, the explanation of this is found in the reflectance spectrum. Figure 19 shows an example of a blue cloth, which also appears bright in NIR radiation (figure 18(b) underneath the glove). Both appearances can be understood easily from reflectance or transmission spectra (figure 19(b)).

3.6. Strange human skin

One of the most spectacular effects of NIR photography happens when recording photographs of people. The skin behaves quite differently in the VIS and NIR ranges, as can be seen in figures 20 and 21.

Human tissue is a highly inhomogeneous material containing many chromophores, blood vessels and light-scattering particles and fibres whose sizes differ appreciably and easily can be larger than the wavelength of incident VIS and NIR radiation. Therefore the optical properties of biological tissue in general, and human skin in particular, must take into account a large number of multiple scattering events and the various layers of the skin behave differently. As a result, the quantitative description of transmitted and reflected radiation is often treated in radiation flux models of the Kubelka–Munk type, see e.g. [40]. In a simplified view, one may

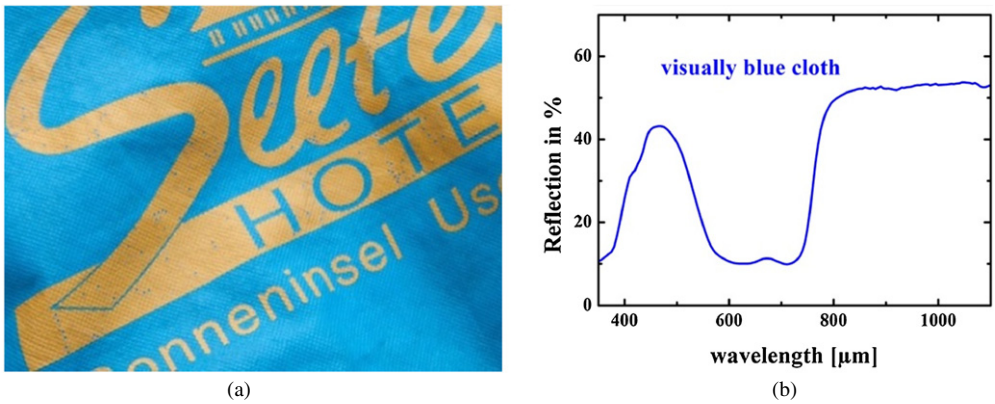

(a) (b)

Figure 19. Blue cloth from a shopping bag (a) is a very good scatterer in the NIR (see figure 18(b) underneath the glove), which is due to its high backscattering properties illustrated in the reflection spectrum (b). Since the material is mostly acting as a diffuse scatterer, the transmission spectrum of the cloth is quite similar to its backscatter spectrum.

Figure 20. Example of an NIR image of the legs of a woman which clearly show the veins below the surface of the skin. These could not be easily seen in the VIS.

argue that skin pigments like melanin become less important toward the NIR and scattering becomes of major importance in deeper skin layers, varying about inversely with wavelength. As a result, the $1/e$ penetration depth of optical radiation can become much larger for NIR radiation than for VIS light. For example, [40] estimated penetration depth values of 90 μm for blue light ($\lambda = 400$ nm), 550 μm for green light ($\lambda = 550$ nm), and 1600 μm for NIR radiation ($\lambda = 1000$ nm). Similarly, maximum depths of visibility of veins were found to range around a few mm in the NIR [41]. This behaviour also can be seen in transmission

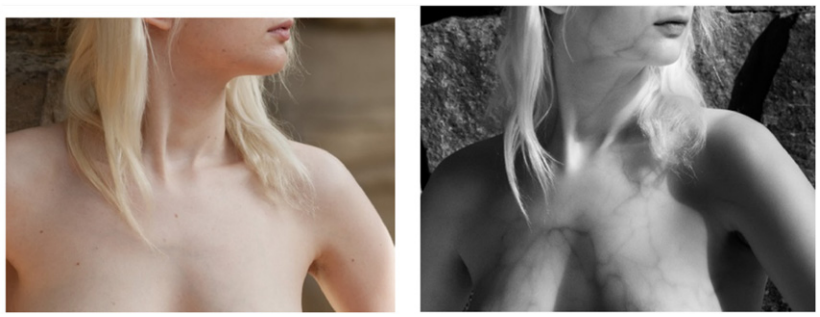

(a) (b)

Figure 21. Example of NIR image of face and part of chest of a woman. Whereas the VIS image (a) shows no blood vessels, the NIR image (b) does so quite spectacularly.

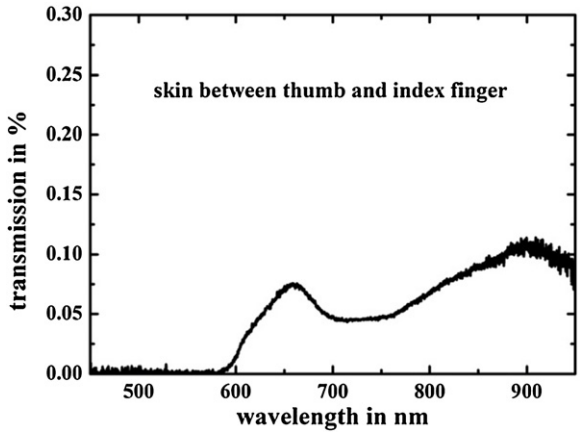

Figure 22. Transmission of about 2 mm skin between thumb and index finger of a human hand. In the VIS, chromophores and haemoglobin absorb efficiently. Besides a small transmission peak in the red part of the spectrum, one easily can see increased transmission towards the NIR.

spectra. As an example, figure 22 depicts a transmission spectrum of an approximately 2 mm thick section of skin, measured between thumb and stretched out index finger with a portable spectrometer. This transmission correlates with the well-known phenomenon that one can easily look through thin skin into a light source and perceive a reddish colour. Please note that the maximum transmission is below 1% here since the detector only registered radiation from a very small solid angle.

Figure 22 and the above discussion can explain the strange effects in NIR photography: images from skin of people recorded with conventional cameras in the VIS may show nothing unusual, whereas the same skin portion recorded as a NIR photograph gives spectacular views of the blood vessels at shallow depth below the surface of the skin. Why is it possible to see such veins much more easily, in particular when illumination has a high NIR content such as direct sunlight (see figure 1) or similar artificial light sources?

From the argument above, we know that NIR radiation may easily penetrate into the depth of low-lying blood vessels. The question is just why they become apparent in the remitted light in the NIR but not so in the VIS range. This cannot be answered easily, since the remitted light

is due first to reflection from the boundary air-to-skin, resulting in a few per cent of reflection, but second and more important here, from the upward-scattered radiation flux from within the skin. It consists of multiply scattered light [41] spectrally modified by absorption processes. The blood vessels have only slight differences in the index of refraction from neighbouring skin tissue (e.g. 1.33 to 1.4); therefore, Fresnel coefficients for the reflection from the tissue–blood boundary are negligibly small (for chosen n-values, e.g., giving a normal reflectivity of only 6×10^{-4}). This means that differences will arise from different absorption properties of blood vessels relative to regular skin tissue. Respective studies in the VIS spectral range have proven that near-surface blood vessels situated below biological tissue can indeed be located by slight differences in their remittance [42], i.e. the radiation scattered backwards out of the sample after multiple scattering processes. The depicted VIS and NIR images show examples where the blood vessels are in deeper regions such that there is no contrast possible for the VIS remitted light since VIS light would be too strongly attenuated before reaching the surface again. However, the NIR radiation, which can penetrate deeper into the skin tissue, has a higher probability of making it back to the surface. In the NIR images, the observable size of the veins most probably is strongly increased, For example, the VIS light study [42] argued that the apparent size had tripled in comparison to the actual vein size for blood vessel depths of around 0.5 mm.

The phenomenon has a very nice application when performed in transmission. It has been used to enhance localization of subsurface blood vessels needed for blood withdrawal in children. The blood vessels are usually located at depths from 1 to several mm and the method worked successfully in hands or wrists and also at the inside of the elbow of children. High power NIR LEDs around $\lambda = 850$ nm were used underneath the puncture sites and images were captured from above. The contrast in the image results from a combination of the scattering of NIR radiation in the tissue and the absorption by haemoglobin in the blood vessels [41] and is best between $\lambda = 850$ and 900 nm.

4. Conclusions

Modern digital cameras and simple optical filters provide an excellent means of observing the otherwise invisible NIR world. This opens up many possible opportunities to teach how simple physics principles can be used to explain the unusual appearance of some everyday objects and scenes. We have given a variety of example images recorded in VIS and NIR light, and shown how measured reflection and transmission spectra can be used to explain the resulting different appearances. Such measurements can be made with relatively low-cost spectrometers that are often available for physics students to experimentally study such phenomena.

References

[1] White L 1996 *Infrared Photography Handbook* (Buffalo, NY: Amherst Media) ISBN-10: 0936262389
[2] Farace J 2006 *Complete Guide to Digital Infrared Photography* (Asheville, NC: Lark Books) ISBN-10: 1579907725
[3] Busch D 2007 *David Busch's Digital Infrared Pro Secrets* (Boston, MA: Thomson Course Technology)
[4] Sandidge D 2009 *Digital Infrared Photography* (New York: Wiley) ISBN: 978-0-470-40521-5
[5] Richards A 2001 *Alien Vision—Exploring the Electromagnetic Spectrum with Imaging Technology* (Bellingham, WA: SPIE Optical Engineering Press)
[6] Karstädt D, Möllmann K P, Pinno F and Vollmer M 2001 There is more to see than eyes can detect: visualization of energy transfer processes and the laws of radiation for physics education *Phys. Teach.* **39** 371–6
[7] Möllmann K-P and Vollmer M 2007 Infrared thermal imaging as a tool in university physics education *Eur. J. Phys.* **28** S37–S50
[8] Vollmer M and Möllmann K-P (ed) 2010 *Infrared Thermal Imaging: Fundamentals, Research and Applications* (New York: Wiley)

[9] Xie C and Hazzard E 2011 Infrared imaging for inquiry-based learning *Phys. Teach.* **49** 368–72
[10] Bochníček Z 2008 An amateur video camera as a detector of infrared radiation *Phys. Educ.* **43** 51–56
[11] Catelli F, Giovannini O and Bolzan V D A 2011 Estimating the infrared radiation wavelength emitted by a remote control device using a digital camera *Phys. Educ.* **46** 219–22
[12] Gross N A, Hersek M and Bansil A 2005 Visualizing infrared phenomena with a webcam *Am. J. Phys.* **73** 986–90
[13] Kuhn J and Vogt P 2012 Diffraction experiments with infrared remote controls *Phys. Teach.* **50** 118–9
[14] Mills A 2012 An inexpensive digital infrared camera *Phys. Educ.* **47** 297–300
[15] Thoms L J, Colicchia G and Girwidz R 2013 Low-cost experiments on infrared phenomena *Phys. Educ.* **48** 16–9
[16] Zetie K 2006 Cheap camera illuminates the infrared *Phys. Educ.* **41** 208
[17] Planinšič G 2004 A photoshoot for food and drink: camera 'sees' more than you think *Phys. Educ.* **39** 32–3
[18] Micklavzina S 2003 Tricks with invisible light *Phys. Educ.* **38** 492–4
[19] Lee E V 2004 Detecting infrared radiation with a phototransistor and an IR filter *Phys. Teach.* **42** 83–5
[20] Huebner J S and Sundaralingam N 1998 Remote controls for infrared experiments *Am. J. Phys.* **66** 544–7
[21] Pursell E E and Kozlowski R 2000 Infrared radiation: Herschel revisited *Phys. Teach.* **38** 559–60
[22] Bochníček Z 2013 Visualization of infrared radiation using thermal sensitive foils *Phys. Educ.* **48** 607
[23] Anderson G P, Clough S A, Kneizys F X, Chetwynd J H and Shettle E P 1986 AFGL atmospheric constituent profiles (0–120 km) *Environmental Research Papers* No. 854, AFGL-TR-86-0110 www.dtic.mil/cgi-bin/GetTRDoc?AD=ADA175173
[24] Bohren C F and Clothiaux E E 2006 *Fundamentals of Atmospheric Radiation* (New York: Wiley)
[25] Greenler R G 1971 Infrared rainbow *Science* **24** 1231–2
[26] Greenler R G 1988 Beyond the (visible) rainbow *Opt. News* **14** 22–4
[27] Mauer C 2009 Measurement of the spectral response of digital cameras with a set of interference filters *Diploma Thesis* University of Applied Sciences Cologne
[28] Bach H and Krause D (ed) 1997 *Thin Films on Glass* (Berlin: Springer)
[29] Wood R W 1910 A new departure in photography *The Century Magazine* **LXXIX** 4 pp 565–72
[30] Finney A 2007 Infrared photography *Focal Encyclopedia of Photography* 4th edn ed M R Peres (Amsterdam: Elsevier) pp 556–62
[31] Finney A 2007 The Wood effect *J. R. Photogr. Soc.* **147** 366
[32] Mecke R and Baldwin W C G 1937 Warum erscheinen die Blätter im ultraroten Licht hell? *Naturwissenschaften* **25** 305–7
[33] Allen W A, Gausman H W and Richardson A J 1973 Willstatter–Stoll theory of leaf reflectance evaluated by ray tracing *Appl. Opt.* **12** 2448–53
[34] Cipar J, Cooley T, Lockwood R and Grigsby P 2004 Distinguishing between coniferous and deciduous forests using hyperspectral imagery *IGARSS 2004: 2004 IEEE Int. Geoscience and Remote Sens. Symp. Proc.* vol 4 pp 2348–51
[35] Hogan J A *et al* 2012 Detection of leaking CO_2 gas with vegetation reflectances measured by a low-cost multispectral imager *IEEE J. Sel. Top. Appl. Earth Obs. Remote Sens.* **5** 699–706
[36] Shaw J A *et al* 2012 Multispectral imaging systems on tethered balloons for optical remote sensing education *J. Appl. Remote Sens.* **6** 063613
[37] Schaul L, Fredembach C and Süsstrunk S 2009 Color image dehazing using the near-infrared *ICIP: Proc. IEEE Int. Conf. on Image Processing* pp 1629–32
[38] Darias-Martin J, Carrillo M, Diaz E and Boulton R B 2001 Enhancement of red wine colour by pre-fermentation addition of copigments *Food Chem.* **73** 217–20
[39] Kamuf W, Nixon A, Parker O and Barnujm G C Jr 2003 Overview of caramel colors *Cereal Food World* **48** 64–69
[40] Anderson R R and Parrish J A 1981 The optics of human skin *J. Invest. Dermatol.* **77** 13–19
[41] Cupera N J *et al* 2013 The use of near-infrared light for safe and effective visualization of subsurface blood vessels to facilitate blood withdrawal in children *Med. Eng. Phys.* **35** 433–40
[42] Kienle A *et al* 1996 Why do veins appear blue? A new look at an old question *Appl. Opt.* **35** 1151–60